ACS APPLIED MATERIALS & INTERFACES

Research Article

www.acsami.org

Mechanical and Transport Properties of Layer-by-Layer Electrospun Composite Proton Exchange Membranes for Fuel Cell Applications

Matthew M. Mannarino,[†,§] David S. Liu,[‡,§] Paula T. Hammond,*[,‡] and Gregory C. Rutledge*[,‡]

[†]Department of Materials Science & Engineering, Massachusetts Institute of Technology, Cambridge, Massachusetts 02139, United States

[‡]Department of Chemical Engineering, Massachusetts Institute of Technology, Cambridge, Massachusetts 02139, United States

Supporting Information

ABSTRACT: Composite membranes composed of highly conductive and selective layer-by-layer (LbL) films and electrospun fiber mats were fabricated and characterized for mechanical strength and electrochemical selectivity. The LbL component consists of a proton-conducting, methanol-blocking poly(diallyl dimethyl ammonium chloride)/sulfonated poly(2,6-dimethyl-1,4-phenylene oxide) (PDAC/sPPO) thin film. The electrospun fiber component consists of poly(trimethyl hexamethylene terephthalamide) (PA 6(3)T) fibers in a nonwoven mat of 60−90% porosity. The bare mats were annealed to improve their mechanical properties, which improvements are shown to be retained in the composite membranes. Spray LbL assembly was used as a means for the rapid formation of proton-conducting films that fill the void space throughout the porous electrospun matrix and create a fuel-blocking layer. Coated mats as thin as 15 μm were fabricated, and viable composite membranes with methanol permeabilities 20 times lower than Nafion and through-plane proton selectivity five and a half times greater than Nafion are demonstrated. The mechanical properties of the spray coated electrospun mats are shown to be superior to the LbL-only system and possess intrinsically greater dimensional stability and lower mechanical hysteresis than Nafion under hydrated conditions. The composite proton exchange membranes fabricated here were tested in an operational direct methanol fuel cell. The results show the potential for higher open circuit voltages (OCV) and comparable cell resistances when compared to fuel cells based on Nafion.

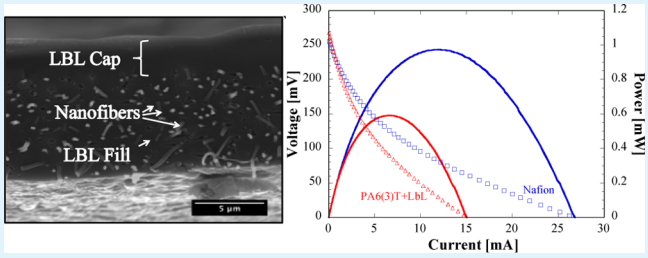

KEYWORDS: *proton conductivity, electrospinning, polyelectrolyte multilayer, membrane mechanics*

1. INTRODUCTION

Improvements to the performance of thin-film solid polymer electrolytes are critical for the advancement of electrochemical energy devices.[1] In recent years, there has been considerable interest in designing more chemically stable and mechanically robust membranes while maintaining high ionic conductivity and low fuel crossover.[2,3] For current state-of-the-art hydrogen and methanol fuel cells, proton exchange membranes (PEMs) comprising perfluorosulfonic acid polymers such as Nafion are the material of choice, primarily because they exhibit superior protonic conductivity, relatively high mechanical integrity, and chemical stability; however, even perfluorosulfonic acid polymers have shown limited device lifetimes due to mechanical degradation.[4,5] One of the main causes of membrane failure is the repeated swelling/deswelling of the membrane during fuel cell operation due to the cycling of temperature and humidity. This cyclic fatigue stress has been shown to weaken the membrane mechanically after as few as a hundred cycles.[6,7] The hydrothermal mechanical behavior of Nafion during swelling has been extensively studied;[5,8,9] there is a significant need to improve upon the current membrane's durability. Many methods have been proposed to improve the mechanical properties of PEMs, such as incorporating Nafion into a polytetrafluoroethylene (PTFE) supporting matrix.[10,11] Other methods of mechanical reinforcement include the incorporation of metal oxides,[12] zirconium phosphates,[13] and carbon nanotubes[14] into Nafion matrices in order to improve PEM lifetime or the overall fuel cell performance.

The continued reliance on Nafion, with its high cost and relatively high fuel crossover, has proven to be a limiting factor for development of direct methanol fuel cells (DMFCs). In recent years, alternative composite polyelectrolyte membranes have been investigated as substitutes for Nafion in PEMs, such as semi-interpenetrating polymer networks (IPNs),[15] sulfonated poly(ether ether ketone)/phenoxy resin (SPEEK/PHR) composites,[16] poly(vinyl alcohol)/sulfonated polyhedral oligosilsesquioxane (PVA/sPOSS) hybrid membranes,[17] and sulfonated polystyrene/poly(vinylidene fluoride) blends compatibilized with block copolymers.[18] More recently, researchers have attempted to fabricate a composite membrane based on sulfonated poly(2,6-dimethyl-1,4-phenylene oxide) (sPPO), reinforced by electrospun and cross-linked bromomethylated

Received: June 8, 2013
Accepted: July 22, 2013
Published: July 22, 2013

   dx.doi.org/10.1021/am402204v | ACS Appl. Mater. Interfaces 2013, 5, 8155−8164

poly(2,6-dimethyl-1,4-phenylene oxide) (cBPPO), for a hydrogen fuel cell.[19] While many of these alternative composite PEMs have shown promising results, there are still concerns regarding their mechanical durability, chemical stability, and/or transport properties that prevent them from widespread use in DMFCs.

In recent reports, we have produced layer-by-layer (LbL)-based PEMs that perform well in hydrogen and direct methanol fuel cells.[20,21] LbL assembly is a versatile nanoscale fabrication technique that allows for the coating of any wettable substrate with a combination of two or more polymers possessing complementary interactions such as oppositely charged functional groups.[22,23] The films can be tuned by adjusting the pH or salt content of the polymer solutions; the thickness per bilayer of films constructed by the LbL method ranges from as small as a few nanometers to over 100 nm. An LbL system composed of poly(diallyl dimethyl ammonium chloride) (PDAC) and sulfonated poly(2,6-dimethyl-1,4-phenylene oxide) (sPPO) has shown particular promise for use in a DMFC. It has the highest ionic conductivity of any LbL assembled system to date, at 70 mS·cm^{-1}, comparable to that of Nafion, while possessing methanol permeability values less than 1/100 that of Nafion. A key weakness of this promising system is that it is mechanically deficient when hydrated.[21,24,25] In fact, many electrostatically assembled polymer membrane systems present the same issues with regard to mechanical integrity.

Electrospun fiber (EF) mats are nonwoven materials with high porosities and high specific surface areas (~1−10 m^2/g).[26,27] A wide range of polymers can be formed into electrospun mats, and it has been shown that the resulting fiber diameters can be controlled during fabrication in the range of 0.1−10 μm, depending on the solution and processing parameters.[28] In addition, we have previously shown that significant improvements in the mechanical response of EF mats can be achieved by thermal annealing, with only modest decreases in porosity of the mats.[29] The spray-assisted LbL process can be used to coat fibers individually throughout the interior of the electrospun mat with the assistance of a vacuum to control the convection of the spray through the mat; in the absence of a vacuum, the spray-assisted LbL process creates a film that can bridge the pores at the surface of the mat, resulting in an asymmetric composite membrane.[25,30] This versatility in fabrication through the combination of LbL assembly and electrospinning allows for the manufacture of PEMs with controllable transport properties. Previously, we demonstrated that the highly selective PDAC/sPPO LbL system could be conformally coated onto electrospun fiber mats and successfully blocks pores, thus producing a stronger membrane with superior methanol resistance when compared to Nafion.[25]

In this work, we manipulate the structure of the underlying electrospun nanofiber scaffold to investigate the effects on the mechanical and functional performance of the composite proton exchange membrane. Thermal annealing of the electrospun fiber mats at temperatures near the glass transition was found to improve the mechanical response and dimensional stability of the coated PEMs. The mechanical durability and hysteretic cycling of the composite membranes were investigated as well as the key transport properties (protonic conductivity and methanol permeability) for a PEM to be used in a methanol fuel cell. The transport properties of the composite systems are controllable by manipulation of the fiber formation and LbL deposition parameters. Complete membrane electrode assemblies (MEAs) were constructed and used to evaluate composite PEM performance in an operational DMFC for comparison to Nafion.

2. EXPERIMENTAL SECTION

2.1. Chemicals. PPO (M_w = 23000) was obtained from Sigma-Aldrich, Inc. PDAC (M_w = 240000) was obtained from Polysciences, Inc. Poly(trimethyl hexamethylene terephthalamide) [PA 6(3)T] was purchased from Scientific Polymer Products, Inc. *N*,*N*-Dimethyl formamide (DMF) was purchased from Sigma-Aldrich and used as received for creating polymeric solutions. PPO was sulfonated as previously reported[21] to yield highly sulfonated sPPO. Magnesium nitrate salt was purchased from Sigma-Aldrich and used as received. An E-Tek gas diffusion layer (GDL) comprising 4.0 mg/cm^2 of 60 wt % HP Pt catalyst on Vulcan XC-72 was used for the cathode side of the membrane electrode assembly (MEA) and an E-Tek GDL comprising 4.0 mg/cm^2 of 80 wt % Pt/Ru catalyst on Vulcan XC-72 was used for the anode side. For the custom ink and wet deposition, 80 wt % Pt/Ru on Vulcan carbon was purchased from the Fuel Cell Store. Nafion DE2020 solution was purchased from Ion Power, Inc., and used as the catalyst binder at 0.8:1 wt. ratio to carbon. Catalyst ink slurry using a 1:1 mixture by volume of 2-propanol:water as solvent was sonicated for 5 min before application. The target catalyst loading was 4.0 mg/cm^2, and the gas diffusion layer was ELAT carbon cloth from the Fuel Cell Store.

2.2. Electrospinning Fiber Mats. As described in a previous report,[29] the electrospinning apparatus consisted of two aluminum disks 10 cm in diameter oriented parallel to each other and separated by a distance of 30 cm. A 22 wt % solution of PA 6(3)T in DMF was pumped through a Teflon tube with a syringe pump (Harvard Apparatus PHD 2000) at a rate of 0.01 mL/min through a 0.040 in. I.D. needle in the top aluminum disk. A high voltage power supply (Gamma High Voltage Research, ES40P) provided 20−24 kV potential to the upper aluminum disk, and the polymer solution jet emitted from the needle was drawn to the bottom grounded disk, where ultrafine fibers of approximately 400 nm diameter were collected. The thickness of the mat (from ~10 to 80 μm) was controlled by the time allowed for deposition. The EF mats were (optionally) annealed in an oven at a specified temperature between 130 and 170 °C for 2 h prior to coating by the spray-LbL method as previously reported.[29]

2.3. LbL Spray Assembly. Samples of EF mats about 100 mm in diameter were first plasma treated in an oxygen atmosphere for 1 min to make the EF mats hydrophilic and to impart an initial negative charge to the fibers (forming carboxylates on the surface).[31] The mats were then placed onto a 75 mm diameter plastic funnel fitted with a steel mesh (2 mm grating) to support the membrane. Sprayed films were fabricated using the same polymer and rinse solutions described previously.[25] For all ES mats 25 μm or thicker, halfway through the desired number of bilayers, the coated mat was flipped over on the steel mesh such that the vacuum was drawn through the opposite side; this was done to provide a more even coating throughout the fiber matrix. The coated fiber mats were then hydrated in deionized water and consolidated in a Carver Hot Press (15 cm × 15 cm platens) at 100 °C and 50 kN for 30 min in order to reduce the remaining pore spaces within the composite membrane. A "capping layer" of LbL film (typically 1 μm thick) was then applied to the composite membrane on both sides by spraying without the vacuum assist to further inhibit methanol crossover. Free-standing LbL films were also assembled on Teflon substrates or polystyrene-coated silicon wafers and gently peeled off after assembly, similar to a previous report.[24]

2.4. Composite Membrane Characterization. Scanning electron microscopy (SEM) images were obtained on a JEOL JSM-6060 scanning electron microscope after coating the composite membranes with roughly 5 nm of Au/Pd. Cross-sectional images were obtained by cryofracturing the composite membranes in liquid nitrogen. Porosities of the fiber mats were determined gravimetrically by cutting out rectangular specimens and measuring the mass and dimensions of the mat sample and converting to porosity. Sample thickness was measured with a Mitutoyo digital micrometer with a constant

measuring force of 0.5 N. Lateral sample dimensions were determined using a digital caliper. The volume and mass of the specimen were then converted to a porosity using the bulk density. The bulk density was estimated as the average value for the polymers used: PA 6(3)T (1.12 g/cm^3), sPPO (1.06 g/cm^3), PDAC (1.04 g/cm^3).

2.5. Mechanical Testing. Uniaxial tensile testing of dry and fully hydrated electrospun fiber mats and composite membranes was performed with a Zwick Roell Z2.5 tensile testing machine using a 2.5 kN load cell. Rectangular specimens were cut to 100 mm × 12.5 mm and extended at a constant crosshead speed of 0.50 mm/s with a 50 mm gauge length (corresponding to a constant strain rate of 0.01 s^{-1}). The thickness of each specimen was determined from the average of three measurements taken along the gauge length with a Mitutoyo digital micrometer at a constant force of 0.5 N. The force-displacement data were converted to engineering stress versus engineering strain using the initial cross-sectional area and gauge length of the test specimen, respectively. Samples defined as "dry" were tested at ambient conditions of 25 °C and approximately 40−45% RH, while samples defined as "hydrated" were conditioned overnight in water and tested while fully saturated with water. Tensile testing under specific humidity conditions was conducted in an EnduraTEC Electroforce 3200 (ELF) with an environmental control chamber. Samples were cut to 4 mm × 30 mm and tested at a constant crosshead speed of 0.12 mm/s with a 12 mm gauge length (corresponding to a constant strain rate of 0.01 s^{-1}). The ELF testing grips were completely enclosed in a stainless steel chamber, which was controlled at 25 °C and 50% RH with a magnesium nitrate salt solution, as confirmed by a humidity gauge. Samples were equilibrated in a humidity chamber before being transferred to the testing chamber, and the chamber allowed to re-equilibrate for 1 min after reaching the desired relative humidity prior to being tested.

Swelling measurements were performed by cutting out approximately 10 mm × 10 mm specimens and measuring the precise length and width using a Mitutoyo digital caliper with 0.01 mm precision. Specimens were then placed in boiling water (maintained at 100 °C) for 2 h, following the specifications set by MacKinnon et al.,[7] before being removed and remeasured using the digital calipers. The linear swelling was then defined as: swelling % = 100% × $(L_s - L_0)/L_0$, where L_0 is the longer of the original length or width (at ambient humidity, 50% RH), and L_s is the corresponding swollen length or width of the specimen.

2.6. Transport Properties. Proton conductivity, unless otherwise noted, was measured in-plane using a custom machined PEEK electrode with two platinum wires spaced 1 cm apart. The samples were immersed in 18.2 MΩ deionized water before drying to ensure the removal of excess ions and then dried and cut into approximately 1.5 cm × 2 cm rectangles and placed on top of a glass slide. The electrode was placed above the PEM specimen and clamped down to ensure good continuous connection between the wires and the sample membrane. Humidity was controlled using a chamber from Electrotech Systems, Inc. Impedance values were determined by electrochemical impedance spectroscopy with a Solartron 1260 impedance analyzer, measuring from 1 MHz down to 1 Hz at room temperature.

Through-plane proton conductivity measurements were made using a two electrode Swagelok cell with two 12 mm diameter aluminum plates as electrodes.[32] The composite membrane testing specimens were soaked in deionized water and cut into 12 mm diameter disks. Excess water was removed from each sample with a laboratory tissue, and the specimen was placed between two 10 mm diameter fine wire meshes to decrease the contact resistance. Impedance values were determined using a Solartron 1260 impedance analyzer as described earlier; the membrane resistance was calculated as the total resistance minus the resistance contribution of the Swagelok cell and the two wire meshes.

Methanol permeability values were determined by using a dual chamber apparatus, where the membrane sample is the separator between pure methanol and water, as described previously.[21] The liquids in both chambers were stirred, and the increase in methanol concentration of the water as a function of time was determined by the changes in the refractive index of the solution using a Waters 2414 refractive index detector.

2.7. Direct Methanol Fuel Cell Testing. The membrane electrode assemblies (MEA) were fabricated by sandwiching a 16 mm diameter circular cut-out composite PEM between two 12 mm diameter GDLs containing catalyst coating and hot-pressing at 135 °C and a force of 5 kN for 5 min using a Carver Hot Press. Two 8 cm × 8 cm square gasket layers (250 μm thick PTFE-coated fiberglass sheets, VWR) were used to align the positions of the PEM and GDL during hot-pressing and to transfer the assembly to the DMFC. The MEAs were then tested using DMFC hardware obtained from Fuel Cell Technologies, Inc. Methanol (10% v/v in water) was fed to the anode at a flow rate of 4 mL/min using a peristaltic pump, and humidified air was supplied to the cathode at 60 mL/min. Polarization curves were generated from a Gamry PCI750 potentiostat connected to the DMFC hardware.

3. RESULTS AND DISCUSSION

3.1. Composite PEM Fabrication. Figure 1 shows a diagram illustrating the main steps of composite PEM fabrication (electrospinning, spray-assisted LbL deposition, hot-pressing, and LbL capping), as well as a representative cross-sectional SEM of a completed composite membrane. The membrane solidity (defined as (1-porosity)) was found to increase up to ∼70−80% with 200−250 bilayers, at which point further increases in solidity with additional bilayers were not observed. To fill the remaining interstices of the fiber matrix (and thus create a denser composite membrane), the coated membranes were hydrated in deionized water and hot-pressed. This process allows the collapse of the remaining pore space between the hydrated, compliant coatings on fibers, thus increasing the overall PEM solidity.

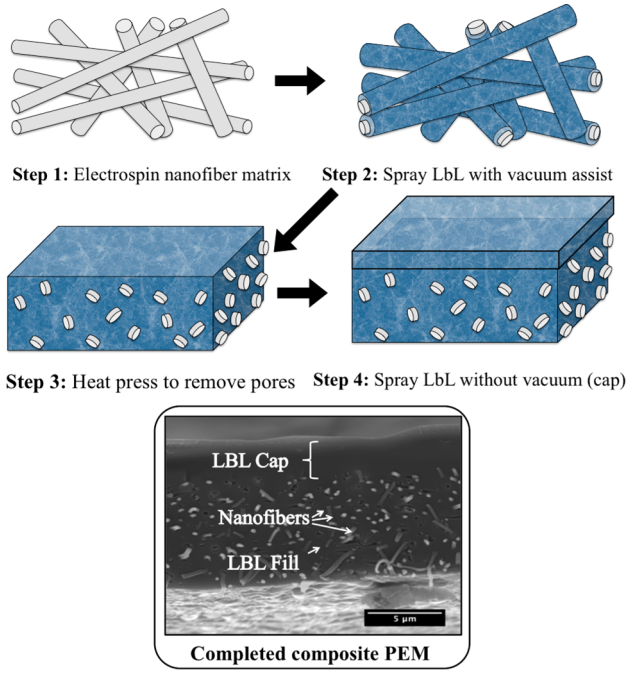

Figure 1. Diagram showing the steps used in fabricating the composite PEM: (1) electrospinning of nanofiber matrix (with optional thermal annealing), (2) spray-coating fibers with LbL polyelectrolytes with vacuum assist, (3) heat pressing membrane to remove voids, (4) coating LbL without vacuum to provide a capping layer to top of PEM. The SEM micrograph is a cross-section of a typical composite PEM. The scale bar of the SEM micrograph is 5 μm.

Thermal annealing of the underlying electrospun fiber matrix at 130, 150, and 170 °C was used to improve the mechanical properties of the composite PEM. Annealing at temperatures close to the glass transition (T_g) of PA 6(3)T was found to increase the mechanical strength while increasing the solidity of uncoated EF mats from about 11−14%, for mats annealed below 150 °C, up to 35% for mats annealed at 170 °C.[29] After coating 200 bilayers of PDAC/sPPO using vacuum-assisted spray-LbL deposition, all membranes plateaued at 68−76% solidity. We hypothesize that the residual porosity was due to closing off of unfilled pores prematurely ("bottle-necking") and nonuniformity of pressure drop through the entirety of the membrane. Hot-pressing of the hydrated membranes was used to push the membrane solidity up to 88−93%, with the EF mats originally annealed at 130 and 150 °C exhibiting the highest overall solidities after fabrication. Data for the solidity of the composite membranes after each step in the fabrication process, as a function of the annealing temperature of the EF mat prior to LbL deposition can be found in the Supporting Information (Figure S1). Although all of the composite membranes exhibit comparable solidities after hot-pressing, the ratio of LbL:EF for the 170 °C thermally annealed fiber mats is much lower than that of the other membranes.

Representative SEM images of the composite PEM at different stages of fabrication are shown in Figure 2. PA 6(3)T

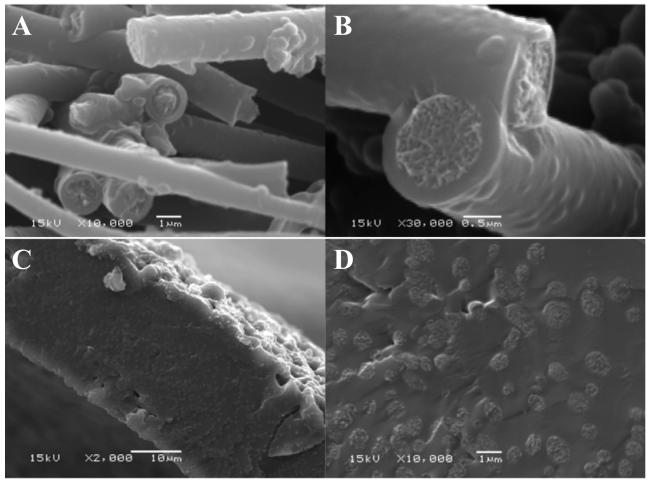

Figure 2. SEM micrograph of ∼800 nm diameter PA 6(3)T fibers coated with 50 bilayers of PDAC/sPPO (A,B). SEM micrograph of composite PEM, consisting of PA 6(3)T fibers whose interstices are completely filled with PDAC/sPPO (250 BLs with vacuum assist) after being hot-pressed while hydrated. Scale bars for (A) and (D) are 1 μm; scale bar for (B) is 0.5 μm; scale bar for (C) is 10 μm.

nanofibers that have been conformally coated with 50 bilayers of PDAC/sPPO are shown in Figure 2A,B; there remains a significant amount of pore space between the coated fibers. SEM micrographs of a cross-section of the hot-pressed composite membranes with 250 bilayers of PDAC/sPPO sprayed with vacuum assist are shown in Figure 2C,D; the LbL film can be seen filling the interstices between the PA 6(3)T fibers due to compression of the hydrated LbL system into the void space during pressing. Before hot-pressing, the composite membrane was an opaque, whitish color; after hydrating and hot-pressing, it turns clear as a result of the elimination of residual air pockets that scatter light.

3.2. Mechanical Properties. We have previously shown that the mechanical properties of the composite LbL-EF membranes in the hydrated state depend primarily on the nonwoven fiber "endoskeleton", while those of the composite membranes in the dry state are stiff and brittle, like the LbL film itself.[25] The mechanical properties of uncoated nanofiber mats have also been investigated extensively and can be controlled by various post-spin treatments.[29,33,34] Annealing of the PA 6(3)T nanofiber mats, in particular, improves the mechanical properties of the EF mats by a factor of 5−6-fold over the as-spun mats. Here we show that these improvements survive hydration and are reflected in the composite PEMs as well.

Under dry conditions, the Young's moduli of the composite membranes range from 383 ± 43 MPa for the composite PEM based on the unannealed PA 6(3)T EF mat, up to 482 ± 71 MPa for the composite PEM based on the EF mat annealed at 150 °C. Yield stresses range from 8.9 ± 3.5 to 12.3 ± 3.3 MPa for these same composite PEMs. The values for Young's modulus and yield stress are comparable to the values for the free-standing PDAC/sPPO film, at 610 ± 113 and 12.8 ± 4.5 MPa, respectively. Even though the Young's moduli and yield stresses of the composite PEMs are greater than those of Nafion, all of the LbL systems exhibit brittle behavior at 25 °C and 50% RH.

In an operational DMFC, the composite PEMs are in a hydrated state; therefore, tensile testing was also conducted on membranes that have been preconditioned in water for 24 h and tested while hydrated. A summary of the improvements to the Young's moduli and yield stresses of the composite PEMs when hydrated as a function of the annealing temperature of the EF mat is shown in Table 1. An increase of up to 5−6-fold in the Young's modulus and yield stress of the hydrated composite PEM can be observed for the composite PEMs as a result of annealing the underlying PA 6(3)T fiber mat. The mechanical properties of the fully hydrated composite LbL-EF PEMs with various temperatures of heat treatment match that of the uncoated PA 6(3)T fiber mats under the same conditions, confirming that the mechanical response of the composite PEM is controlled by the underlying electrospun mat. At 150 °C heat-treatment, the mechanical properties of the hydrated composite PEM are comparable to that of hydrated Nafion N112, with Young's moduli of 80.2 ± 9.9 and 74.3 ± 5.7 MPa, and yield stresses of 3.39 ± 0.37 and 5.56 ± 0.22 MPa, respectively.

Figure 3 compares the data for engineering stress vs engineering strain for a typical composite membrane annealed at 150 °C vs Nafion in the hydrated state; included as well, for reference, are curves for a hydrated uncoated 150 °C heat-treated PA 6(3)T fiber mat and for a free-standing LbL film. When hydrated, the free-standing LbL film becomes plasticized and pliable, thus losing most of its mechanical integrity. The yield stress drops to ∼0.1 MPa and the Young's modulus drops to 1−2 MPa. Figure 3 shows that when coated onto the heat-treated PA 6(3)T electrospun fiber scaffold, the composite membrane exhibits the superior mechanical response of the underlying thermally treated EF mat. At low strains (<0.05 mm/mm), the mechanical response of the composite membrane is nearly identical to that of the hydrated Nafion membrane and maintains its integrity through the plastic deformation region (>0.05 mm/mm).

The failure mechanisms of the coated fiber mats in both the dry and hydrated cases were observed during mechanical testing. In the dry case, cracking occurs along the LbL surface,

Table 1. Summary of Mechanical and Swelling Properties of Composite PEM at 25 °C

	Young's modulus (100% RH) [MPa]	yield stress (100% RH) [MPa]	strain at break (50% RH) [mm/mm]	linear swelling[a] [mm/mm]	hydration stability factor[b] (HSF)	hysteresis[c] (1 swelling cycle) (100% RH) [%]
PDAC/sPPO film	1.70 ± 0.95	0.11 ± 0.04	0.06 ± 0.02	0.16 ± 0.02	0.34 ± 0.11	N/A
As-spun + LbL	36.1 ± 5.1	1.07 ± 0.14	0.10 ± 0.02	0.05 ± 0.01	1.84 ± 0.35	47.5 ± 6.3
130 °C HT + LbL	52.1 ± 10.8	1.69 ± 0.10	0.09 ± 0.01	0.04 ± 0.01	1.97 ± 0.31	36.8 ± 5.6
150 °C HT + LbL	80.2 ± 9.9	3.39 ± 0.37	0.09 ± 0.01	0.03 ± 0.01	2.76 ± 0.37	37.0 ± 5.2
170 °C HT + LbL	197.7 ± 54.2	6.51 ± 0.63	0.07 ± 0.01	0.03 ± 0.01	2.64 ± 0.37	39.2 ± 5.4
Nafion N112	74.3 ± 5.7	5.56 ± 0.22	1.56 ± 0.15	0.36 ± 0.04	4.28 ± 0.40	62.9 ± 3.9

[a]Subjected to boiling water (100 °C) for 2 h. [b]Ratio of strain at break [mm/mm] to linear swelling [mm/mm]. [c]Each sample extended to its corresponding linear swelling strain.

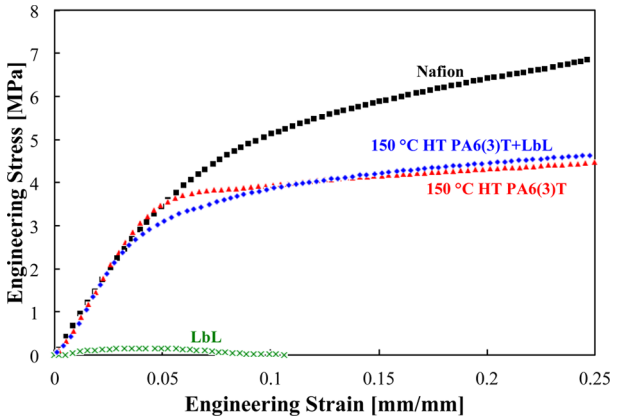

Figure 3. Representative stress–strain plots for hydrated membranes of: Nafion (black squares), 150 °C heat-treated PA 6(3)T nanofiber mat (red triangles), free-standing LbL film (green ×s), and the composite of PA 6(3)T and LBL, using 150 °C heat-treated electrospun mat (blue diamonds).

exposing the underlying electrospun mat. In the hydrated case, the polyelectrolyte coating is able to deform with the rest of the mat without cracking due to the ductile behavior of the LbL films when hydrated; this ductility was also observed in bare film testing. SEM micrographs of the fracture plane for composite membranes after tensile testing in both "dry" conditions and "wet" conditions are presented in Figure 4. The breaking mechanism for the dry samples is brittle fracture, as indicated by the minimal plastic deformation of the specimen before breaking and the very smooth conchoidal fracture (normal to the applied tension) (Figure 4A). The breaking mechanism for the wet samples is ductile rupture; the wet membrane exhibits significant necking and the fiber matrix deforms plastically before rupture, yielding a very rough fracture surface (Figure 4B). Consequently, the spray coated fiber mats exhibit greater toughness in the hydrated state relative to the free-standing PDAC/sPPO films and are comparable to commercial proton exchange membranes such as Nafion.

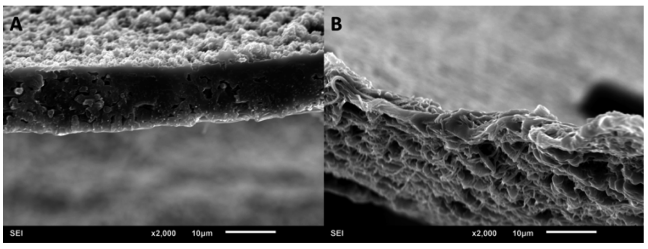

Figure 4. Representative SEM micrographs of composite LbL-electrospun fiber membrane fracture surfaces: (A) "dry" membrane fracture plane indicating brittle fracture mechanism, (B) "wet" membrane fracture plane showing thinning and plastic deformation during ductile rupture. The scale bar for each image is 10 μm.

3.3. Swelling Behavior. In an operational fuel cell, the PEM undergoes repeated swelling and deswelling cycles, which can decrease significantly the lifetime of the membrane.[9,35] Perfluorosulfonic acid (PFSA)-based proton exchange membranes, such as Nafion, exhibit substantial swelling in water. Repeated hydration cycling often leads to mechanical failure and fracture as a result of membrane thinning and pinhole formation;[9,36] therefore, PEMs that swell less offer some advantages in a fuel cell due to their potential for increased service lifetime. Figure 5 shows that the composite membranes

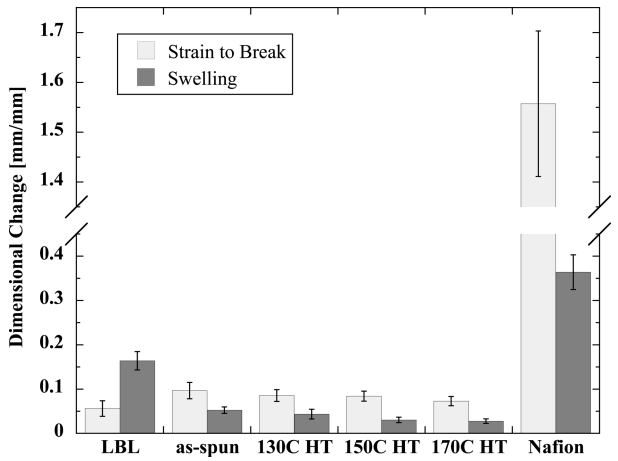

Figure 5. Dimensional change in the strain to break (at 50% RH) and linear swelling of composite PEMs and Nafion.

fabricated in this work have significantly greater dimensional stability than both Nafion and the pristine LbL film during a swelling experiment under the same conditions. We hypothesize that the significant decrease in linear swelling for the composite PEM is due to constraint of the LbL film within the electrospun fiber matrix; the LbL film is electrostatically bound to the fiber surfaces and is unable to expand freely because the film is mechanically weaker than the electrospun fibers. This hypothesis explains why the linear swelling decreases with increasing annealing temperature of the underlying EF mat.

dx.doi.org/10.1021/am402204v | ACS Appl. Mater. Interfaces 2013, 5, 8155–8164

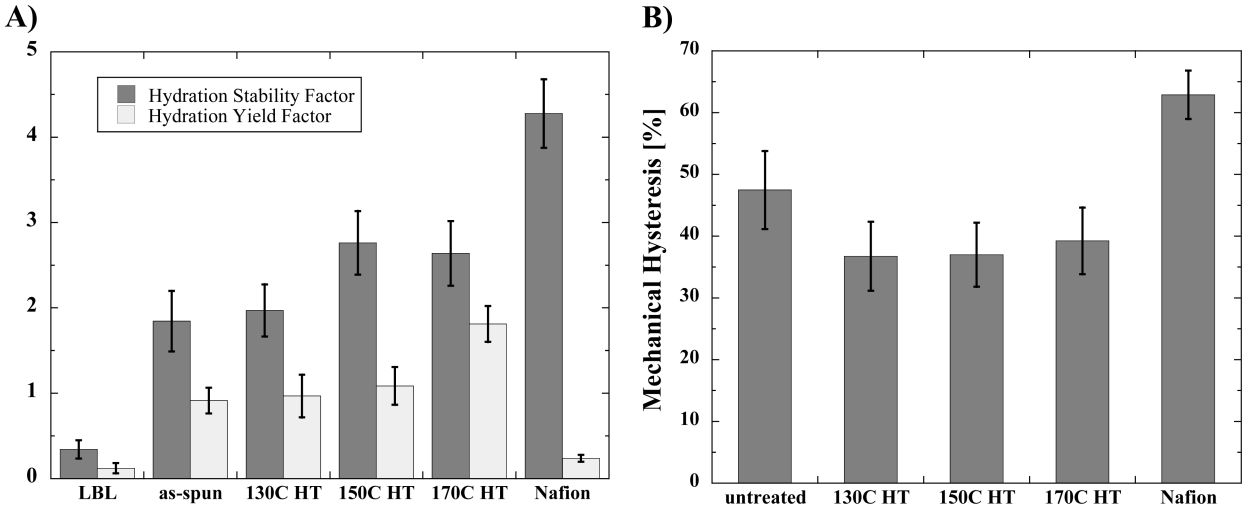

Figure 6. (A) Comparison of hydration stability factor and hydration yield factor for the free-standing LbL film, composite PEMs made with EF mats annealed at different temperatures, and Nafion. (B) Comparison of the mechanical hysteresis for composite PEMs made with EF mats annealed at different temperatures and Nafion.

Figure 5 also shows a comparison of the tensile strain-to-break of the PEMs at 50% RH and 25 °C. The composite membranes exhibited both a moderate increase in the strain to break at 50% RH (0.06 mm/mm for the free-standing LbL to 0.10 mm/mm for the composite system), and a more than 3-fold decrease in the linear swelling (from 0.17 mm/mm for the free-standing LbL to 0.03−0.05 mm/mm for the composite PEM), compared to the pristine LbL film. The linear swelling strains of all of the LbL systems were found to be significantly lower than Nafion, which swelled to 0.36 ± 0.04 mm/mm, nearly an order of magnitude larger than the composite PEMs. A summary of the strain to break and linear swelling properties can be found in Table 1.

The mechanical durability of a PEM in a hydrated fuel cell is directly linked to its tensile strain to break and its linear swelling in the same direction after exposure to liquid water. Membranes undergo significant swelling when humidified and may fail mechanically if membrane stresses experienced during hydration cycling exceed the tensile strength of the membrane; therefore, larger membrane breaking strains are desirable. The hydration stability factor is a metric that was proposed recently for characterizing the likelihood that a membrane can withstand repeated humidity cycling;[7] it is defined as:

$$\text{HSF} = (\text{strain at break}[\text{mm/mm}](25°\text{C, 50\% RH})) / (\text{linear swelling}[\text{mm/mm}](100°\text{C in } H_2O)) \quad (1)$$

This metric has proven to be a convenient measure for assessing various membranes and for predicting their relative durability in the accelerated mechanical humidity cycling test. Figure 6A shows the HSF of the composite membranes as well as the HSF of the free-standing LbL film and of Nafion. A value of HSF < 1 indicates that the membrane is not robust enough to survive even one humidity cycle, which highlights the weakness of the free-standing PDAC/sPPO film, whose HSF is 0.34 ± 0.11. All of the composite LbL-EF membranes are seen to have HSF values that are 5−6 times larger than that for the free-standing LbL and only ∼30% or so less than Nafion; these results indicate that the composite LbL-EF PEMs possess sufficient mechanical integrity to withstand humidity cycling in an operational fuel cell.

The comparable values of HSF for the composite PEMs and Nafion suggest that the LbL-EF membranes may exhibit humidity fatigue cycling lifetimes similar to Nafion; however, the HSF does not fully capture the significant advantage of the dimensional stability (reduced linear swelling) of the composite PEMs in this work. A comparison of the single load-unload stress−strain curves for Nafion and the composite LbL-EF membrane under extension can be found in the Supporting Information (Figure S2A). The membranes are extended up to a total strain equivalent to its linear swelling deformation in boiling water. It is important to note that the strain reached by Nafion upon swelling (∼0.36 mm/mm after 2 h in water at 100 °C) extends well beyond the yield point (∼0.08 mm/mm at 25 °C, RH = 50%) of Nafion. A membrane that is repeatedly deformed beyond the yield point loses its mechanical integrity irreversibly, increasing the likelihood of mechanical failure within an operational fuel cell.[33]

To better evaluate the extent of the irreversible deformation a membrane would experience with each swelling cycle, we propose the following "hydration yield factor", which we define as

$$\text{hydration yield factor} = (\text{yield strain}[\text{mm/mm}](25°\text{C, 50\%RH})) / (\text{linear swelling}[\text{mm/mm}](100°\text{C in } H_2O)) \quad (2)$$

If the hydration yield factor is greater than 1, then the swelling occurs mostly within the elastic regime and strains associated with repeated cycling should be mostly recoverable; however, if the hydration yield factor is less than 1, then the sample deforms plastically during each cycle; the more the ratio is below one, the greater the permanent deformation exhibited by the membrane during hydration cycling. All of the composite PEM's exhibit hydration yield factors of ∼1 or higher (1.09 ± 0.22 for the 150 °C annealed sample), indicating that the strains induced in the membranes by swelling are equal to or slightly below the yield point, and thus mostly recoverable, as shown in Figure 6B. The hydration yield factor of Nafion is found to be 0.24 ± 0.04, which corresponds to large plastic (unrecoverable) deformation after each swelling cycle.

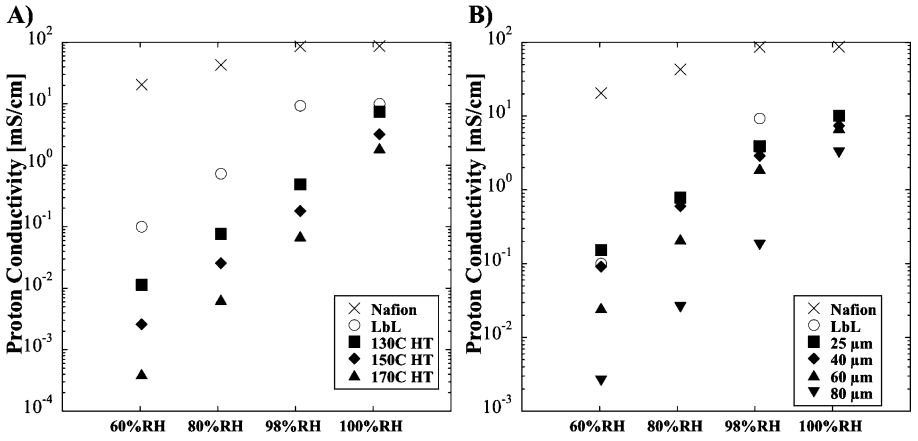

Figure 7. Humidity dependence of the in-plane proton conductivity of (A) the composite PEMs assembled on various thermally treated EFMs (80 μm thick before annealing) and free-standing LbL film and (B) the proton conductivity for different composite PEM thickness (150 °C heat-treated samples). The in-plane proton conductivity of Nafion (N112) is included for reference.

To quantify the energy loss during a swelling cycle, the mechanical hysteresis for a single cycle of loading and unloading (up to the measured swelling strain) was determined for each sample and compared to that of Nafion (Supporting Information Figure S2B). The area contained between the load−unload curves is an indication of the work performed on the membrane with each swelling cycle; Nafion exhibits significantly larger hysteretic losses compared to the LbL-EF membranes. A quantitative comparison of the percent of mechanical hysteresis for each type of PEM is shown in Figure 6B. All of the composite LbL-EF membranes exhibit lower percent mechanical hystereses relative to that of Nafion. The composites of 130 and 150 °C heat-treated PA 6(3)T and LbL exhibit the lowest hysteretic losses, at 36.8 ± 5.6% and 37.0 ± 5.2%, respectively, compared to 62.9 ± 3.9% for Nafion. The greater dimensional stability and lower mechanical hysteresis indicate the potential for longer operational lifetimes of the composite LbL-EF proton exchange membranes relative to Nafion.

3.4. Transport Properties. In-plane conductivities of the composite PEMs assembled using the various thermally treated PA 6(3)T electrospun scaffolds and of the free-standing LbL-deposited film were measured to quantify their dependence on humidity (see Figure 7A). All of the composite PEMs and the pristine LbL film show similar humidity dependence; the proton conductivity improves by approximately an order of magnitude with every 20% increase in the relative humidity, indicating that the proton conduction mechanism of the LbL films is not significantly affected by the assembly method or by the supporting scaffold. The PA 6(3)T electrospun mats (80 μm thick) annealed at 130 °C yielded composite PEMs with a protonic conductivity several times higher than those annealed at 150 or 170 °C. The slight porosity decrease of the fiber mats is not enough to explain the significant drop in ion transport with the higher annealing temperatures. This difference in the conductivity is most likely due to difficulty in coating mats comprising merged fibers and weld points, which are believed to exacerbate bottle-necking of the spray-LbL before complete filling of pore space. Lower total resistances and a reduction of bottle-necking can be achieved by utilizing thinner proton exchange membranes in DMFCs and in the composite LbL-EF PEMs. Figure 7B shows the effect of using electrospun mats of various thicknesses (80, 60, 40, and 25 μm thick before coating and pressing) for fabrication of the composite PEM. All of these PA 6(3)T mats were annealed at 150 °C. The thinner membranes exhibited increased protonic conductivity due to more complete impregnation with polyelectrolytes; when fully hydrated, the thinnest membrane (25 μm) exhibits protonic conductivity comparable to that of a pure LbL film.

To observe the effect of adding the capping layer on conductivity, the through-plane and in-plane conductivities were measured for uncapped and capped PEMs (see Supporting Information Figure S3). While the in-plane conductivity of the capped PEM (7.7 ± 0.4 mS/cm) showed a marked, 4-fold increase over that of the uncapped PEM (1.6 ± 0.1 mS/cm), the through-plane conductivity of the capped PEM (7.0 ± 0.3 mS/cm) was comparable to that of the uncapped PEM (6.9 ± 0.4 mS/cm). We hypothesize that the uncapped composite PEM had a low in-plane conductivity due to proton transport occurring along the length of the electrospun fibers, which are randomly aligned, and that the large increase in the in-plane conductivity after the addition of the capping layer was the result of the conduction through the capping LbL film. Conversely, the uncapped composite PEM exhibited a high through-plane conductivity because the LbL films were already well connected through the thickness of the fiber matrix as a result of the vacuum-assisted LbL deposition process and the subsequent hot-pressing. The capping process does not alter significantly the through-plane ionic conductivity of the mat. Note that despite the anisotropic morphology of the capped composite PEM, the conductivity through-plane and in-plane are quite similar. This is in contrast to Nafion membranes, which exhibit through-plane conductivities between $^1/_3$ and $^1/_4$ of their in-plane conductivities.[4]

While the through-plane proton conductivity of the composite PEM provides an indication of the membrane's ability to sustain high currents in a fuel cell, its methanol permeability ultimately determines its potential use for DMFC applications. Lower crossover limits fuel loss and permits the use of a higher methanol feed concentration. This in turn leads to a higher overall cell voltage, power density, and efficiency. In the context of DMFCs, "selectivity" is defined as the ratio of proton conductivity to methanol permeability and is a useful metric for predicting the performance of a PEM.[7] Protons and methanol have similar molecular transport mechanisms in sulfonic acid-containing PEMs. As a consequence, it is generally difficult to improve membrane selectivity significantly, even with substantial modifications to the membrane's ion content,

Table 2. Summary of Transport Properties of Composite PEMs

membrane	through-plane proton conductivity[a] (σ) [mS/cm]	MeOH permeability ($P \times 10^8$) [cm^2/s]	selectivity ($S = \sigma/P \times 10^8$) [mS·s/cm^3]
PA6(3)T + PDAC/sPPO (~10 μm cap/30 μm) [this work]	7.0	9.7	0.72
Nafion N112[4]	26	198	0.13
sulfonated poly(styrene-*b*-ethylene-*r*-butadiene-*b*-styrene) block copolymer[37]	23	82	0.28
phosphotungstic acid/poly(vinyl alcohol) composite[38]	6	45.4	0.13
Nafion/poly(vinyl alcohol) blend[39]	20	65	0.31
PVOH/PVP blend[40]	1.4	10	0.14
SPEEK/cyclodextrin[41]	48	76	0.63

[a]tested at 100% RH.

water content, or polymer chemistry, architecture, or morphology.[4] LbL assembled PDAC/sPPO films exhibit methanol permeabilities 2 orders of magnitude lower than that of Nafion due to the light cross-linking between PDAC and sPPO. It is therefore possible to decrease the methanol crossover of the composite PEM significantly (by capping) while maintaining a reasonable through-plane conductivity. Table 2 shows a summary of the through-plane proton conductivity, methanol permeability, and calculated selectivity of the composite PEM from this work, compared with Nafion and highly selective composite PEMs reported in the literature. The capped composite PEM was made from an 18 μm thick EF mat that was thermally treated at 130 °C, coated by the vacuum assisted spray LbL method, and subsequently capped with 5 μm of PDAC/sPPO on both sides. The resultant PEM had a through-plane conductivity $^1/_4$ that of Nafion (7 vs 26 mS/cm) and methanol permeability 20 times lower than that of Nafion (9.7 vs 198 × 10^{-8} cm^2/s). The result is a selectivity five and a half times greater than that of Nafion (7.2 vs 1.3 × 10^7 mS·s/cm^3) and greater than that of all the highly selective composite PEMs listed in Table 2. Taking into consideration the thickness of the composite membrane (30 μm) relative to that of the Nafion membrane typically used in a DMFC (180 μm), the composite PEM's conductance (conductivity/thickness) is 60% higher than that of Nafion, and its permeance (permeability/thickness) is still 3.4 times lower than that of Nafion.

3.5. DMFC Performance. Despite the attractive characteristics of the composite PEM, fabrication of a membrane electrode assembly (MEA) using the composite PEM proved to be a challenge. This difficulty was traced to incomplete bonding of the PEM to the electrode during MEA assembly. The difficulty in determining optimum hot-pressing conditions for adhesion of the PEM to the catalyst layers was exacerbated by the incompatible thermal expansion and swelling of the composite PEM versus the catalyst, which has a Nafion binder, especially upon drying. The Pt catalyst-coated GDL (cathode side) was found to adhere well to the LbL-EF composite PEM after MEA hot-pressing; however, the Pt/Ru catalyst-coated GDL (anode side) was found to delaminate frequently from the PEM, leading to increased cell resistances and greatly reduced catalyst activation. This problem has been observed previously with other Nafion-free PEMs.[42] Cross-sectional SEM micrographs of the MEA showing the delamination of the Pt/Ru catalyst side can be found in the Supporting Information (Figure S4).

Several techniques to remedy the MEA delamination were attempted; these included adjusting the hot-pressing conditions (temperature, time, wet or dry PEM), adding a thin layer of Nafion paint as binder, coating catalyst directly onto the PEM, or even synthesizing a custom batch of Pt/Ru catalyst slurry using PDAC/sPPO as the polymer binder. A summary of several of the various MEA construction methods and catalysts used are shown in Table 3 along with the resultant cell resistances and comments on whether methanol penetrated through the membrane. In each case, the MEA exhibited higher cell resistances and/or higher methanol crossover than expected. However, some trends were observed to reduce cell resistances. Hot-pressing was observed in all situations to improve contact and, on average, reduced resistances by half. However, hot-pressing while wet led to increased methanol crossover, which we believe was due to failure of the capping layer. Wet assembly of the cell (either by depositing the ink on the membrane or by using wet membranes) further improves contact and prevents delamination (upon drying), but the membranes again tend to exhibit methanol crossover. Use of excess Nafion paint helped reduce the methanol crossover but not completely. These techniques for improving connection typically have little effect in Nafion based systems, further proof that it is the difference in properties of the composite membrane (i.e., mechanical properties, swelling, and flow

Table 3. Summary of MEAs

membrane condition	anode catalyst[a]	hot press	area-normalized cell resistance[b] [Ω·cm^2]	comments
wet	none	n/a	0.43	resistance of membrane alone
dry flat	Pt/Ru (E-TEK)	no	20.65	fuel blocking
dry flat	Pt/Ru (E-TEK)	yes	12.31	fuel blocking
dry flat	Pt/Ru (wet deposit)	no	11.80	fuel break-through
dry flat	Pt/Ru (wet deposit)	yes	6.01	fuel break-through
wet	Pt/Ru (E-TEK)	no	7.96	fuel break-through
wet	Pt/Ru (custom ink)	no	5.21	fuel break-through
wet	Pt/Ru (E-TEK)	yes	3.47	3× Nafion paint, reduced break-through
dry flat	Pt (E-TEK)	yes	3.01	fuel blocking

[a]Pt (E-TEK) used as cathode catalyst for all MEAs. [b]Defined as the cell resistance times the effective area of the cell (1.13 cm^2)

behavior) versus Nafion that is responsible for the high resistances.

Since we were not successful in integrating the Pt/Ru catalyst into the MEA containing the composite LbL-EF PEM, an alternative system consisting of Pt-catalyst coated GDL sandwiched around both sides of the PEM was used to obtain a relative measure of the DMFC performance. The activation energy of methanol oxidation with Pt catalyst is higher than that with Pt/Ru catalyst, resulting in lower fuel efficiency; however, the PEM transport should be unaffected. Comparison of the overall performance of this MEA with the composite PEM to that of an MEA constructed using Nafion and the same Pt(anode)/Pt(cathode) catalyst assembly provides a useful measure of the relative operational DMFC performance. Figure 8 shows voltage−current polarization curves as well as power

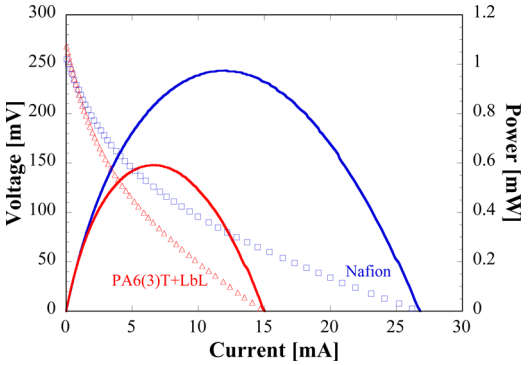

Figure 8. V−I polarization and power density curves for Nafion and PA6(3)T + LBL composite membrane using Pt catalyst for both the anode and cathode GDL in 10 wt % methanol/water mixture.

density curves for a 100 μm thick Nafion PEM and a 25 μm thick LbL-EF composite PEM in a DMFC using 10 wt % methanol in water as the fuel and tested at 25 °C. The MEA with composite PEM exhibits comparable open circuit voltage (OCV) to the MEA with Nafion (270 vs 257 mV), indicating that methanol is blocked as efficiently by the thinner composite PEM. The MEA with composite PEM also draws a current of 5.8 mA at 100 mV, compared to 9.4 mA at 100 mV for the MEA with Nafion. Even with the Pt catalyst, the total cell resistance was greater than expected based on the sum of the area-normalized resistances in series for the individual components (electrode, PEM, charge collector) (3.01 $\Omega \cdot cm^2$ measured vs ~0.6 $\Omega \cdot cm^2$ estimated from components alone). From this, we conclude that the contact resistances between components are high, which we attribute to poor adhesion between the PEM and electrode, indicating that the PEM adhesion to the electrode was still not optimal. It is possible that the DMFC performance of the composite PEM could be further improved with the development of a custom catalyst and binder system for optimized compatibility with the composite PEM, but this is beyond the scope of the current study.

4. CONCLUSIONS

Composite membranes of highly conductive LbL films, and electrospun fiber mats were fabricated and characterized for mechanical strength and electrochemical selectivity. To create a proton-conducting, fuel-blocking layer and to fill in the void space throughout the porous electrospun fiber matrix, the spray-LbL assembly method with and without vacuum was used to form LbL films rapidly. These membranes consist of highly selective poly(diallyl dimethyl ammonium chloride)/sulfonated poly(2,6-dimethyl-1,4-phenylene oxide) (PDAC/sPPO) thin films. The mechanical properties of the spray coated electrospun fiber mats are shown to improve with increasing temperature of thermal annealing of the underlying electrospun scaffold. The composite PEMs exhibited a Young's modulus of 80.2 MPa and a yield stress of 3.39 MPa when the EF mat was annealed at 150 °C, comparable to the mechanical properties of Nafion under the same testing conditions. Modifications to the mechanical response of the composite PEM were achieved by thermal treatment of the underlying EF mat. The composite PEMs swelled less than Nafion under hydration cycling; the greater dimensional stability means lower mechanical hysteresis under hydration cycling, which promises longer operational lifetimes. The composite PEM also exhibited through-plane proton conductivity as high as 7 mS/cm at 100% RH and methanol permeability as low as 9.7×10^{-8} cm^2/s, indicating a membrane selectivity of 7.2×10^7 $mS \cdot s/cm^3$; this is over five times greater than the selectivity of Nafion. The composite proton exchange membranes were tested in an operational direct methanol fuel cell. These results show the potential for higher OCVs (270 vs 257 mV) and comparable cell resistances when compared to Nafion when using Pt/Pt catalyst for both the anode and the cathode.

■ ASSOCIATED CONTENT

Supporting Information

Data and plots of membrane solidity as a function of thermal annealing of the EF mat, tensile fracture mechanism, mechanical hysteresis, and catalyst delamination. This material is available free of charge via the Internet at http://pubs.acs.org

■ AUTHOR INFORMATION

Corresponding Author

*For P.T.H.: phone, +1 617 258 7577; fax, +1 617 253 8757; E-mail, hammond@mit.edu; address, Massachusetts Institute of Technology, 77 Massachusetts Avenue, Room 76-553, Cambridge MA 02139, United States. For G.C.R.: phone, +1 617 253 0171; fax, +1 617 324 3127; E-mail, rutledge@mit.edu; Massachusetts Institute of Technology, 77 Massachusetts Avenue, Room E17-504D, Cambridge MA 02139 United States.

Author Contributions

§M.M.M. and D.S.L. contributed equally.

Notes

The authors declare no competing financial interest.

■ ACKNOWLEDGMENTS

We thank Jonathon Harding for assistance preparing catalyst inks, Diego Giraldez for help measuring the through-plane conductivities, Prof. Mary C. Boyce for valuable discussions, and the David H. Koch Institute for Integrative Cancer Research at MIT and the MIT Institute of Soldier Nanotechnology for use of facilities. Funding for this work was provided by the Masdar Institute, the U.S. Army through the Institute for Soldier Nanotechnologies (ISN) under AR-OW911NF-07-D-0004 and Samsung Advanced Institute of Technology.

DEDICATION

We dedicate this paper to the memory of Officer Sean Collier for his caring service to the MIT community and for his sacrifice.

REFERENCES

(1) De Brujin, F. *Green Chem.* **2005**, *7*, 132−150.
(2) Ulbricht, M. *Polymer* **2006**, *47*, 2217−2262.
(3) Chalk, S. G.; Miller, J. F. *J. Power Sources* **2006**, *159*, 73−80.
(4) Deluca, N. W.; Elabd, Y. A. *J. Polym. Sci., Part B: Polym. Phys.* **2006**, *44*, 2201−2205.
(5) Mauritz, K. A.; Moore, R. B. *Chem. Rev.* **2004**, *104*, 4535−4585.
(6) Lai, Y.-H.; Mittelsteadt, C. K.; Gittleman, C. S.; Dillard, D. A. *J. Fuel Cell Sci. Technol.* **2009**, *6*, 021002.
(7) MacKinnon, S. M.; Fuller, T. J.; Coms, F. D.; Schoenweiss, M. R.; Gittleman, C. S.; Lai, Y.-H.; Jiang, R.; Brenner, A. M. In *Encyclopedia of Electrochemical Power Sources*; Elsevier Science: New York, 2010; pp 741754
(8) Silberstein, M. N.; Pillai, P. V.; Boyce, M. C. *Polymer* **2011**, *52*, 529−539.
(9) Silberstein, M. N.; Boyce, M. C. *J. Power Sources* **2011**, *196*, 3452−3460.
(10) Liu, F. Q.; Yi, B. L.; Xing, D. M.; Yu, J. R.; Zhang, H. M. *J. Membr. Sci.* **2003**, *212*, 213−223.
(11) Nouel, K. M.; Fedkiw, P. S. *Electrochim. Acta* **1998**, *43*, 2381−2387.
(12) Chalkova, E.; Fedkin, M. V.; Wesolowski, D. J.; Lvov, S. N. *J. Electrochem. Soc.* **2005**, *152*, A1742−A1747.
(13) Yang, C.; Costamagna, P.; Srinivasan, S.; Benziger, J.; Bocarsly, A. B. *J. Power Sources* **2001**, *103*, 1−9.
(14) Liu, Y.-H.; Yi, B.; Shao, Z.-G; Xing, D.; Zhang, H. *Electrochem. Solid-State Lett.* **2006**, *9*, A356−A359.
(15) Chikh, L.; Delhorbe, V.; Fichet, O. *J. Membr. Sci.* **2011**, *368*, 1−17.
(16) Cai, H.; Shao, K.; Zhong, S.; Zhao, G.; Zhang, G.; Li, X.; Na, H. *J. Membr. Sci.* **2007**, *297*, 162−173.
(17) Chang, Y.-W.; Wang, E.; Shin, G.; Han, J.-E.; Mather, P. T. *Polym. Adv. Technol.* **2007**, *19*, 535−543.
(18) Piboonsatsanasakul, P.; Wootthikanokkhan, J.; Thanawan, S. *J. Appl. Polym. Sci.* **2008**, *107*, 1325−1336.
(19) Yun, S.-H.; Woo, J.-J.; Seo, S.-J.; Wu, L.; Wu, D.; Xu, T.; Moon, S.-H. *J. Membr. Sci.* **2011**, *367*, 296−305.
(20) Farhat, T. R.; Hammond, P. T. *Adv. Funct. Mater.* **2005**, *15*, 945−954.
(21) Argun, A. A.; Ashcraft, J. N.; Hammond, P. T. *Adv. Mater.* **2008**, *20*, 1539−1543.
(22) Decher, G. *Science* **1997**, *277*, 1232−1237.
(23) Hammond, P. T. *Adv. Mater.* **2004**, *16*, 1271−1293.
(24) Ashcraft, J. N.; Argun, A. A.; Hammond, P. T. *J. Mater. Chem.* **2010**, *20*, 6250−6257.
(25) Liu, D. S.; Ashcraft, J. N.; Mannarino, M. M.; Silberstein, M. N.; Argun, A. A.; Rutledge, G. C.; Boyce, M. C.; Hammond, P. T. *Adv. Funct. Mater.* **2013**, *23*, 3087−3095.
(26) Doshi, J.; Reneker, D. H. *J. Electrost.* **1995**, *35*, 151−160.
(27) Rutledge, G. C.; Fridrikh, S. V. *Adv. Drug Delivery Rev.* **2007**, *59*, 1384−1391.
(28) Fridrikh, S. V.; Yu, J. H.; Brenner, M. P.; Rutledge, G. C. *Phys. Rev. Lett.* **2003**, *90*, 144502.
(29) Mannarino, M. M.; Rutledge, G. C. *Polymer* **2012**, *53*, 3017−3025.
(30) Krogman, K. C.; Lowery, J. L.; Zacharia, N. S.; Rutledge, G. C.; Hammond, P. T. *Nature Mater.* **2008**, *8*, 512−518.
(31) Pappas, D.; Bujanda, A.; Demaree, J. D.; Hirvonen, J. K.; Kosik, W.; Jensen, R.; McKnight, S. *Surf. Coat. Technol.* **2006**, *201*, 4384−4388.
(32) Guyomard, D.; Tarascon, J. M. *J. Electrochem. Soc.* **1992**, *139*, 937−948.
(33) Pai, C.-L.; Boyce, M. C.; Rutledge, G. C. *Polymer* **2011**, *52*, 6126−6133.
(34) Silberstein, M. N.; Pai, C.-L.; Rutledge, G. C.; Boyce, M. C. *J. Mech. Phys. Solids* **2012**, *60*, 295−318.
(35) Silberstein, M. N.; Boyce, M. C. *J. Power Sources* **2010**, *195*, 5692−5706.
(36) Borup, R.; Meyers, J.; Pivovar, B.; Kim, Y. S.; Mukundan, R.; Garland, N.; Myers, D.; Wilson, M.; Garzon, F.; Wood, D.; Zelenay, P.; More, K.; Stroh, K.; Zawodzinski, T.; Boncella, J.; McGrath, J. E.; Inaba, M.; Miyatake, K.; Hori, M.; Ota, K.; Ogumi, Z.; Miyata, S.; Nishikata, A.; Siroma, Z.; Uchimoto, Y.; Yasuda, K.; Kimijima, K. I.; Iwashita, N. *Chem. Rev.* **2007**, *107*, 3904−3951.
(37) Kim, B.; Kim, J.; Jung, B. *J. Membr. Sci.* **2005**, *250*, 175−182.
(38) Li, L.; Xu, L.; Wang, Y. *Mater. Lett.* **2003**, *57*, 1406−1410.
(39) Deluca, N.; Elabd, Y. *J. Power Sources* **2006**, *163*, 386−391.
(40) Huang, Y. F.; Chuang, L .C.; Kannan, A. M.; Lin, C. W. *J. Power Sources* **2009**, *186*, 22−28.
(41) Yang, T.; Liu, C. *Int. J. Hydrogen Energy* **2011**, *36*, 5666−5674.
(42) Jung, H.-Y.; Cho, K.-Y.; Sung, K. A.; Kim, W.-K.; Park, J.-K. *J. Power Sources* **2006**, *163*, 56−59.